

# Strain Sensitive Polyurethane Nanocomposites Reinforced with Multiwalled Carbon Nanotubes

Daowei Ding<sup>1</sup>, Huige Wei<sup>1,2</sup>, Jiahua Zhu<sup>1</sup>, Qingliang He<sup>1</sup>, Xingru Yan<sup>1</sup>,  
Suying Wei<sup>2,\*</sup>, and Zhanhu Guo<sup>1,\*</sup>

<sup>1</sup>Integrated Composites Laboratory (ICL), Dan F. Smith Department of Chemical Engineering,  
Lamar University, Beaumont, TX 77710, USA

<sup>2</sup>Department of Chemistry and Biochemistry, Lamar University, Beaumont, TX 77710, USA

## ABSTRACT

Conductive elastomeric polyurethane (PU) nanocomposites reinforced with multiwall carbon nanotubes (MWCNTs) for the applications of strain sensor purpose have been synthesized via an *in situ* surface-initiated-polymerization (SIP) method. The morphology of the nanocomposites with a variety of loadings of MWCNTs was investigated by scanning electron microscopy (SEM) and the corresponding chemical structures were studied by Fourier Transform Infrared Spectroscopy (FT-IR). Uniformly distributed MWCNTs were observed at different loadings, i.e., 1.0, 3.0 and 5.0 wt%. Improvements of thermal stability arising from the reinforcing MWCNTs in the nanocomposites were also observed from the test result of thermal gravimetric analysis (TGA). The values of dielectric property were observed to be in direct proportion to the MWCNTs loadings from 2 to  $2 \times 10^6$  Hz and a unique negative permittivity was achieved in the nanocomposites with the highest MWCNTs loading of 10.0 wt% at lower frequency range from 2 to  $2 \times 10^2$  Hz. Electrical conductivity study reveals that the resistance of the fabricated films decreased from the magnitude of  $10^{10}$  to  $10^3 \Omega$  with increasing the MWCNTs loadings from 1.0 to 10.0 wt%. The nanocomposites displayed a good response of the conductivity change to the varying strain in the cyclic strain test, indicating a promising potential for strain sensor applications.

**KEYWORDS:** Elastomer, Polyurethane, MWCNT, Strain Sensor.

## 1. INTRODUCTION

The synthesis and utility of conductive strain sensors have attracted significant importance and interests from both academic and industrial fields for their promising potentials in not only non-live applications such as interactive electronics, implantable medical devices but also bio-live fields in robotic systems with human-like sensing capabilities applications.<sup>1–5</sup> Previous researches conclusion indicate that various materials can be utilized as the base matrixes of strain sensor, such as silicone,<sup>6</sup> ZnSnO<sub>3</sub> nanowires,<sup>7</sup> polypropylene<sup>8</sup> and so on. Elastomers like Vistamaxx 6102FL (VM1, ethylene content 16 wt%, propylene 84%) and Vistamaxx 6202FL (VM2, ethylene content 15 wt%, propylene 85%) reinforced by polyaniline, carbon nanofibers and single-walled carbon nanotubes have also been reported, respectively.<sup>9,10</sup> Generally, high conductivity and quick-precise response are key parameters for achieving strain sensors of desirable properties.<sup>11</sup> Parallely, the durability is also a critical property for strain

sensors since they are usually employed as long term or even semi-permanent parts in various equipments.<sup>1</sup>

Since its first discovery,<sup>1,2</sup> remarkable emphasis and attentions had been raised to carbon nanotubes (CNTs) for their excellent electrical conductivity,<sup>13</sup> outstanding mechanical<sup>14</sup> and unique thermal properties.<sup>15</sup> From the point of chemical structure differences, CNTs are mainly divided into two categories: single-walled carbon nanotube (SWCNTs) and multi-walled carbon (MWCNTs). Due to a much broader radius distribution and significant enhancement in Young's modulus via increasing the layer,<sup>16,17</sup> multi-walled carbon nanotube (MWCNTs) have been studied for various applications.<sup>11,18–21</sup>

Polyurethane (PU), due to its unique property as a commercial matrix base for many nanocomposites, has been widely studied in different fields such as coatings, paints, structural materials, elastomers and adhesives.<sup>22–24</sup> A combination of MWCNTs and PU had been studied in versatile fields. For instance, the combination of CNTs and PU has been utilized to improve the tensile strengths in mimicking the stiffness of natural tissues.<sup>25</sup> SWCNTs/PU was reported as strain measurement via strain paint corresponding to the spectral shifts of the nanotube near-infrared fluorescence peaks when the strains were applied.<sup>26</sup>

\*Authors to whom correspondence should be addressed.  
Emails: zhanhu.guo@lamar.edu (Z. G.), suying.wei@lamar.edu (S. W.)  
Received: 5 January 2014  
Accepted: 12 February 2014

The outstanding performance of microwave absorption from SWCNTs/PU nanocomposites resulted in its more broad applications in EMI shielding field.<sup>27</sup> However, the combination of PU and MWCNT in various nanoparticle loadings have rarely been studied for strain sensor area considering PU belongs to one type of elastomeric materials.<sup>28,29</sup> The major challenge would be the response speed, conductivity of the materials, the cycle period of the materials that can last during an industrial working condition and some other difficulties to overcome.

In the present work, a series of MWCNTs/PU nanocomposites with 1.0, 3.0, 5.0 and 10.0 wt% loading of MWCNTs were synthesized via a surface-initiated-polymerization (SIP) method.<sup>30</sup> The morphology, FTIR (structures), thermal and dielectric properties were characterized. Completed polymerization has been obtained and good dispersion of MWNTs has been observed. Resistance-conductive property corresponding to the applied cyclic strain force is studied as well.

## 2. EXPERIMENTAL DETAILS

### 2.1. Materials

Tetrahydrofuran (THF, 99%) was purchased from Fisher Scientific. MWCNTs (SWeNTSMW 200X, average diameter: 10.4 nm; average length: 4.3  $\mu\text{m}$ ) were provided by SouthWest NanoTechnologies, Inc. The raw materials for the preparation of polyurethane contained three parts: A (polyurethane STD-102, containing organotin-tanate), B (two-part monomers: diol and diisocyanate) and C (containing aliphatic amine, parachlorobenzotrifluoride and methyl propyl ketone in a liquid base), were supplied by PRCDesoto international, Inc. Part A and part C were applied as the accelerator and catalyst, respectively. All chemicals were used as received without any further purification. The procedure of synthesizing polyurethane is shown in Scheme 1.

### 2.2. Preparation of MWCNT/PU Sample

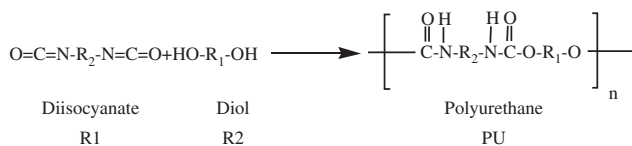
The MWCNTs/PU nanocomposites with a series of loadings were fabricated by a surface-initiated-polymerization (SIP) method. In a brief introduction, the synthesis procedures are as follow: MWCNTs that are specified weights were added to part B, the two-part monomers liquid (11.2 g) for overnight wetting to assure the dispersion. Then the nanoparticle and the two part liquid mixture was mechanically stirred for 15 min to obtain a better dispersion of MWCNTs. Part C (2 g) and part A

(1.8 g) were then introduced to the solution afterward followed by the mechanical stirring for 15 another minutes. When the suspension solution gradually became viscous, the solution was casted on a wafer carrier tray mold (Diameter: 69.95 mm, thickness: 4.25 mm) to form an evenly-balanced thin film. The casted solutions were cured in room temperature for seven days. The solid samples were obtained and then were further polished to avoid the random dent on the surface during the drying period. After that the round-shape sample was cut to a rectangle shape with the dimension of 43 mm length, 4 mm width and 0.6 mm average thickness. Before the strain sensor tensile test, the rectangle-shaped samples were given a permanent elongation to avoid the uneven deformation that may affect the tensile-resistance combined test results. This elongation value was set as from original 43 mm to final 80 mm, which percentile is from 100 to 186%.

### 2.3. Characterizations

The morphology was studied by a JEOL field emission scanning electron microscope, JSM-6700F. The chemical functional groups were analyzed via Fourier Transform infrared spectroscopy (FT-IR) spectrometer coupled together with an accessory in attenuated total resistance (ATR) (Bruker Inc. Vector 22) in the range from 4000 to 500  $\text{cm}^{-1}$  at a 4  $\text{cm}^{-1}$  resolution. The dielectric properties of MWCNTs/PU nanocomposites were performed by a LCR meter (Agilent E4980A) with the accessory of dielectric test fixture (Agilent, 16451B), and the carrying on range was between  $2 \times 10^6$  Hz. The property of thermal stability of MWCNTs/PU was investigated by thermo gravimetric analysis (TGA, TA Instrument TGA Q-500) in the temperature range from 25 to 650  $^{\circ}\text{C}$  and the heating ratio was 10  $^{\circ}\text{C}/\text{min}$  under the gas condition of air and nitrogen, respectively.

The conductivity and resistance when performed the cyclic strain and recover was studied with the combination of a tensile test machine (ADMET tensile strength testing system 610) and a current monitoring instrument (Keithley 2400 SourceMeter. The parameters of tensile tests were controlled via a digital working station (MTESTQuattro) with MTESTQuattro<sup>®</sup> Materials Testing and Running Software. The strain cyclic performance was carried out following the American Society for Testing and Material (ASTM, 2002, standard D882). The rectangular composite films were clamped on the tensile test clamped and was provided a specialized speed force to stress and recovered by the same speed. Figure 2(a) shows the applied strain/recovery setting up. The sample was covered with a conductive copper tape (CU-35C, 3M) at each end, which was clamped with alligators to provide a 4.99–5.00 V source voltage from Keithley 2400 SourceMeter. In the meantime, the current variation during the stretch and recovery process was measured and recorded by the same voltage supplier. This current live monitor could



**Scheme 1.** Two monomers in part B and the formation of polyurethane.

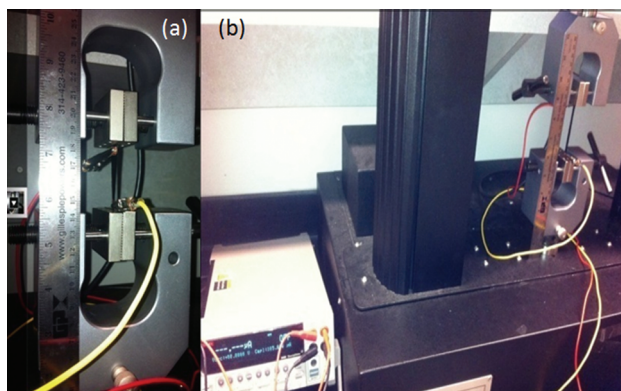


Fig. 1. Tensile test setting configuration.

record the current change from  $10^{-10}$  to  $10^{-2}$  A, which corresponds to a resistance of  $10^2$  up to  $10^{10}$   $\Omega$ . The crosshead strain speed was set as 500 mm/min and the sample test cycle was set as 1000 cycles. Before cyclic tensile test, the film samples were given a permanent elongation of 186.04% to avoid the unexpected deformation, which may affect the obtained results. The above setting configuration and basic physical situation was show in Figure 1.

### 3. RESULTS AND DISCUSSION

#### 3.1. Structure and Morphology

##### 3.1.1. SEM

The surface section cracks of the composite film were demonstrated in Figure 2. In order to study the internal structure, the synthesized MWCNTs/PU composite films were frozen under the atmosphere of liquid nitrogen as the cross section of the fraction areas were more convenient to be observed under this situation.

The dots on those images represent that the dispersion of MWCNTs in polyurethane matrix. At lower loading, the dots were not too many from the images while with the increasing of MWCNTs loading, the dots became into some line-shape tubes, which represent unbroken MWCNTs. And under the SEM test condition, the samples were not as easy to wrack as the lower loading ones. This phenomenon was much more obvious when it come to the 5% MWCNTs/PU. A huge amount of tube-shapes MWCNTs were observed in some part of the product. And the unbroken MWCNTs were marked in tube-shape, which indicated the stronger interaction between MWCNTs with PU. Also, since the total MWCNTs loading had increased, the broken MWCNTs percentage would showed more than that in lower loading nanocomposites. The well dispersion could also be achieved from these images and the dispersion of lower MWNTs loading seems more random than higher MWCNTs loadings. This can be explained that the lower loading of MWCNTs/PU, the less inner action between each other. And when the loading rose up, more and more MWCNTs would interact with the matrix and entangled with itself. Besides, PU is usually considered

as high viscosity materials, which could further prevent even dispersions of the MWCNTs. This structure character was the principal reasonable explanation and can be used to clear the atmosphere that occurred in the following investigations. Besides, for the MWCNTs/PU synthesized films, since there were no phase separations atmosphere occurred, the compatibility between MWCNTs and PU was proved, which was correspond to the previous SWCNTs/PU composites study for their cross-link structure.<sup>15</sup>

##### 3.1.2. FT-IR

The chemical structures of the nanocomposites were analyzed by FT-IR. Figure 3 shows FT-IR spectra of the MWCNTs, pure PU, 1% MWCNTs/PU, 3% MWCNTs/PU, and 5% MWCNTs/PU. Consist with the previous results, no significant peaks were observed for MWCNTs,<sup>31</sup> and therefore all the peaks shown in the composites are mainly attributed to the PU base. A broad peak appeared at  $3364\text{ cm}^{-1}$  indicated the vibration of functional group of  $-\text{NH}$ .<sup>32</sup> The peaks between  $3000$  and  $2600\text{ cm}^{-1}$  are the characteristic bonds contributing from the symmetric and asymmetric stretching of  $-\text{CH}$  in  $-\text{CH}_2$  and  $\text{CH}_3$ .<sup>33</sup> The peak at  $2919\text{ cm}^{-1}$  corresponds to the stretching vibrations of  $-\text{CH}_2$  functional groups while the  $2846\text{ cm}^{-1}$  peak illustrates the stretching of chemical bonds of  $-\text{CH}$  in  $-\text{CH}_3$  groups, respectively.<sup>33,34</sup> The chemical bond vibration occurred at  $1697\text{ cm}^{-1}$  represented the  $-\text{C}=\text{O}$  functional groups.<sup>35</sup> The absorption at  $1638\text{ cm}^{-1}$  corresponds to the urea linkage<sup>36</sup> and the peak at  $1231\text{ cm}^{-1}$  indicates the  $-\text{C}-\text{O}$  functional groups existing in the composites.<sup>35</sup> The characteristic peak of diisocyanate around  $2270\text{ cm}^{-1}$  peak could not be observed in the composite, indicating a completed polymerization of diol and diisocyanate during the curing process.<sup>37,38</sup>

##### 3.1.3. Dielectric Properties

The dielectric properties of the pure PU and MWCNTs/PU nanocomposites were studied by a LCR meter. Figures 4(A)–(C) depicts the real permittivity ( $\epsilon'$ ), imaginary permittivity ( $\epsilon''$ ), and dielectric loss ( $\delta$ ) as a function of frequency in the range of  $20$  to  $\times 10^6$  Hz, respectively. In Figure 4(A), significant enhancement in the  $\epsilon'$  is clearly seen from the composites when compared to the results of pure PU, and  $\epsilon'$  increases with the increasing of MWCNTs loadings in the composites. In low frequency, the composites exhibit a  $\epsilon'$  in a magnitude of  $10^3$  for 1.0 wt% MWNTs and  $10^4$  for 2.0 and 3.0 wt% MWNTs, respectively. Similar phenomenon had been observed from several presvious researches in poly(ethylene glycol),<sup>39</sup> polyaniline doped with  $\beta$ -naphthalene sulphonic acid,<sup>40</sup> carbon nanotube network.<sup>41</sup> These results can be address as the following reason. When the conductive materials doped in the composite, the capability of electron localization and delocalization of the composites was enhanced. The high value of  $\epsilon'$  is due to the Maxwell–Wagner–Sillars effect, where charge carriers can be accumulated

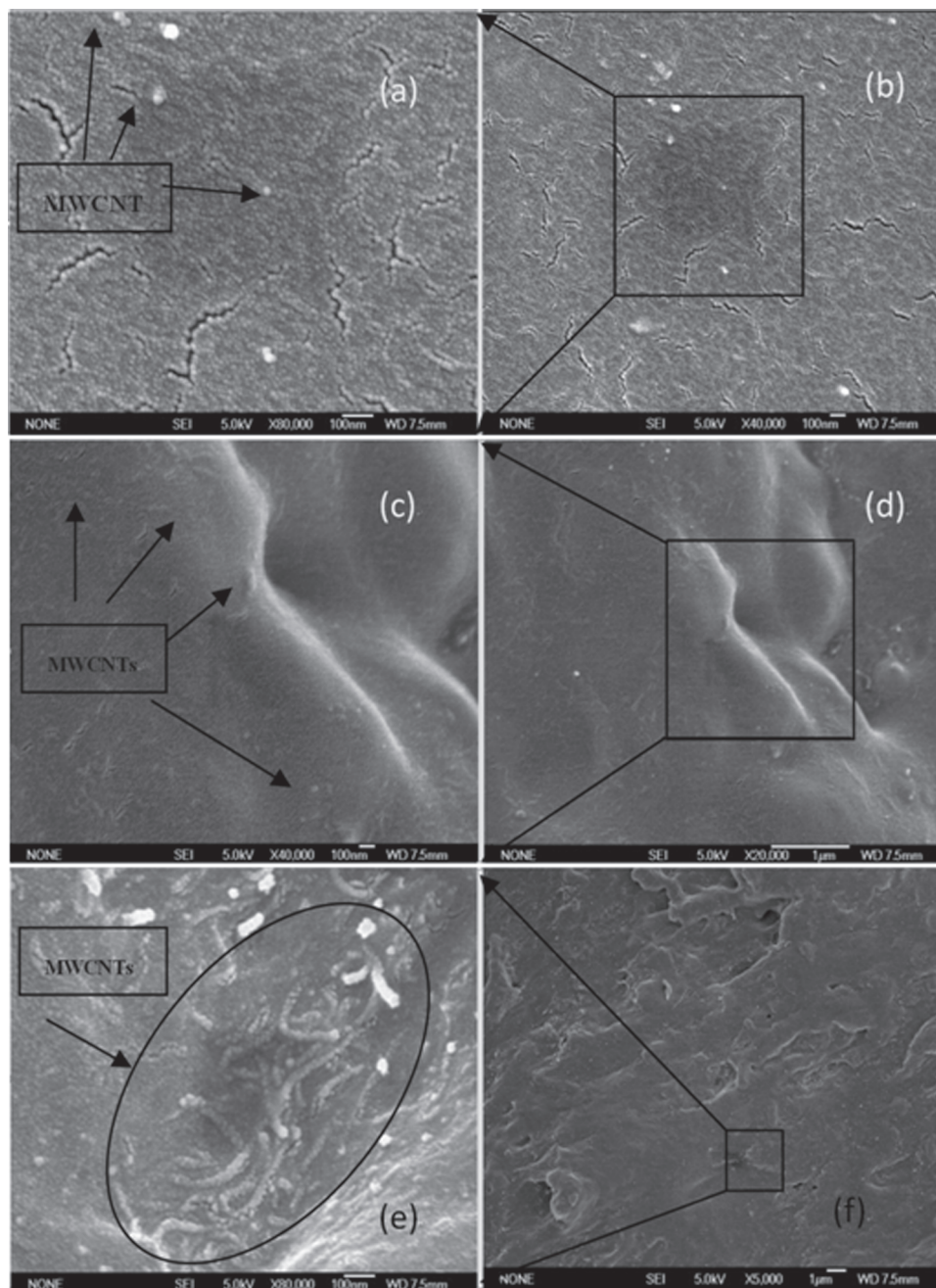


**Fig. 2.** SEM microstructure of (a) and (b) 1.0% MWCNTs/PU, (c) and (d) 3% MWCNTs/PU, (e) and (f) 5% MWCNTs/PU.

at the internal interfaces under an electric field.<sup>42</sup> At the same time, the  $\epsilon'$  decreases with increasing the frequency, which is due to the localization effect. At high conductive nanomaterials loadings, the insulated PU which were “physically wrapped” on the MWCNTs surface became thinner and were not strong enough to keep the charge carriers of the MWCNTs.<sup>43</sup> This phenomenon may also has another reason that the hindrance to the migrations of polarized segment, for instance, atoms, dipolar group, bonds and space charges between the interfaces under a specified external field, where the internal force was the

major consumer of the absorbed energy during the orientation of polarized species.

The free electrons and the scattering dispersion of electrons during the movements attribute to the above phenomena as well.<sup>44</sup> And the more MWCNTs loaded on PU matrix, the decrease of it was larger at the final high frequency; the real permittivity of 5% MWCNTs/PU is the least stable product among the rest products from the point of decreasing real permittivity. Higher reduced value of real permittivity from 3% MWCNTs/PU and 5% MWCNTs/PU were achieved from the graph. This is because that higher

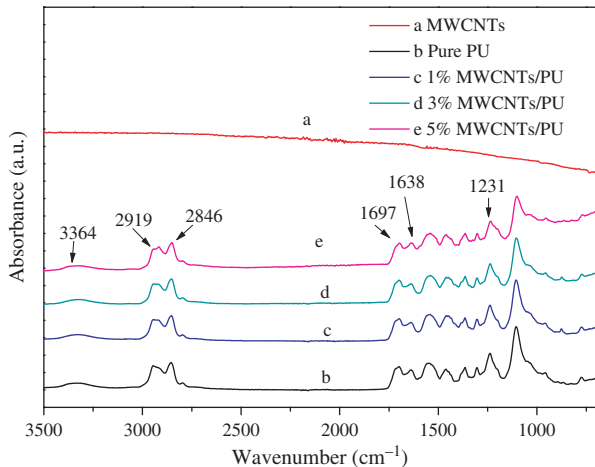


**Fig. 3.** FT-IR spectra of (a) MWNTs, (b) pure PU, (c) 1% MWNTs/PU, (d) 3% MWNTs/PU and (e) 5% MWNTs/PU.

loading of MWCNTs dispersion can carry more electrons and the PU has less interaction to hold the electrons corresponding to the loading, and the free-moving electron here is larger than higher loading ones. So the inner structure is more flexible corresponding to external electric field. This indicated that the constructed nanostructure is easily affected by the external electric field frequency disturbance especially when a moderate frequency adding to the product even though a seemingly-strong interaction had been visualized from previous SEM results. This phenomenon was also observed from the nanocomposites of carbon nanofiber loaded on elastomers (VMI,2).<sup>9</sup>

It is also interesting to acquire negative real permittivity during the sample test of 10% MWCNTs/PU at low frequency while at higher frequency the negative data disappeared, which was not shown here. This phenomenon had already been observed in plenty formal studies such as polypyrrole/Tungsten oxide metacomposites,<sup>45</sup> Magneto resistive polyaniline-magnetite nanocomposites,<sup>46</sup> carbon nanostructure-derived polyaniline metacomposites,<sup>10</sup> polyaniline/Barium Titanate nanocomposites<sup>47</sup> nanopolyaniline/epoxy hybrid<sup>48</sup> and so on. Among these studies existence of negative permittivity are due to the continuous conductive network of the base matrixes, which is defined as percolation phenomenon.<sup>9</sup> So the 10% MWCNTs/PU occurred negative data also indicates the behavior of percolation phenomena. This effect is majorly because that higher loading MWCNTs results in the formation transition of PU and the loaded MWCNTs performed a long-range connection among the MWCNTs.<sup>9</sup> The higher loading introduced plenty of active interfaces between conductive MWCNTs and nonconductive polymer matrix PU and this is another reason for the percolation phenomenon.

Figure 4(B) shows the imaginary permittivity of all the fabricated products. This part is more stable than that in the real permittivity section. Corresponding to  $\epsilon'$ ,  $\epsilon''$  also decreased when frequency was at a high level. From

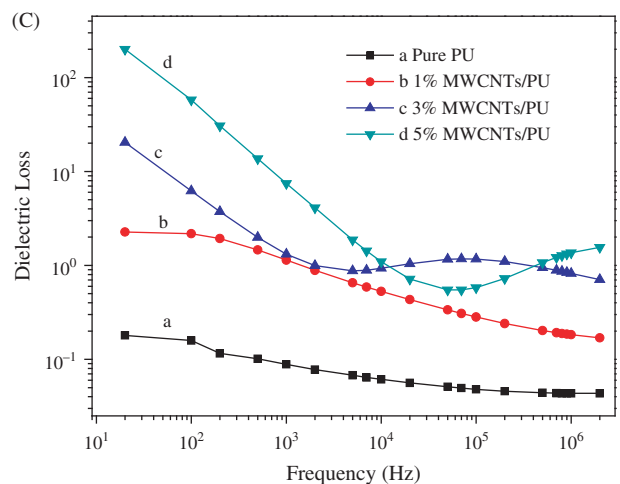
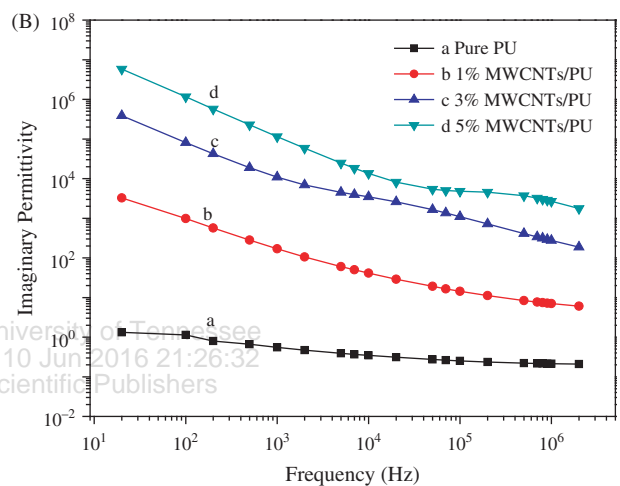
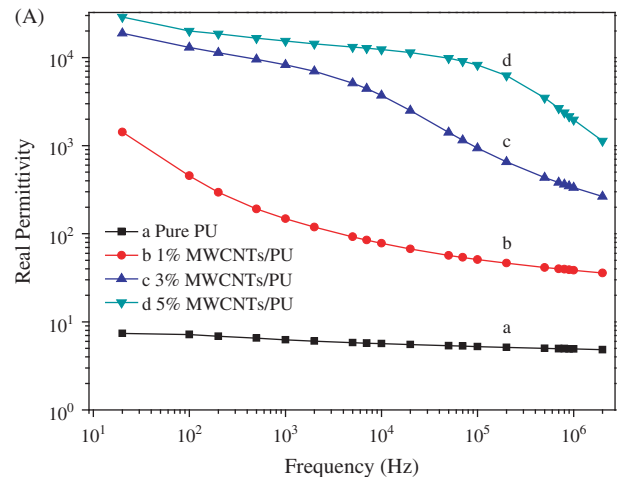


**Fig. 4.** (A) Real Permittivity, (B) imaginary Permittivity, and (C) dielectric loss of the pure PU and the composites.

the definition of the complex permittivity<sup>49</sup> and imaginary permittivity,<sup>50</sup>

$$\epsilon^*(\omega) = \epsilon'(\omega) - j\epsilon''(\omega) \quad (1)$$

$$\epsilon''(\omega) = \frac{\sigma_{0,\text{ion}}}{\epsilon_0(\omega)^\alpha} \quad (2)$$

Where  $j = -I^{1/2}$ ,  $\omega = 2\pi f$ , donates the angular frequency of the supplied electric field,  $\sigma_{0, \text{ion}}$  is the dc ionic conductivity. The imaginary permittivity is attributed by conductivity of materials. That is why in the following section the conductivity also increased together with the MWCNTs loading, i.e., the conductivity is in proportion to the imaginary permittivity. Similar relaxation phenomenon was also observed in this section.

Figure 4(C) illustrates the dependence of the dielectric loss ( $\tan \delta$ , where  $\tan \delta = \varepsilon''/\varepsilon'$ ) as a function of frequency. The dielectric loss of all samples are well corresponded to the principle of permittivity, which is, the dielectric loss increased along with the increase loading of MWCNTs. Moreover, at the lower section of frequency the dielectric loss decreased regularly. However, for 5% MWCNTs/PU, the  $\tan \delta$  decreased dramatically among the frequency range from 2 to  $10^5$  Hz, and after that the dielectric loss began to increase and finally reached stable. 3% MWCNTs/PU also achieved stable dielectric loss at high frequency. This result also correspond to the delocalization of the nanocomposite and less ability of keeping electrons of the base matrix, indicating that the polymer matrix and the loading materials have been seriously impressed by the random dispersion and flexible structure between MWCNTs and PU.

### 3.1.4. Electrical Conductivity

Figure 5 shows resistance trend of the MWCNTs/PU composites. The resistance was greatly reduced from  $2 \times 10^{10}$  to  $2.4 \times 10^5 \Omega$  when the MWCNTs loading was increased from 1.0 comparing to 3% by over 5 orders of magnitude. The conspicuous results demonstrate a significant improvement of the conduct property, which has a strong relation to the dispersion of the conductive fillers in polymer base matrix.<sup>9, 21, 51, 52</sup> And this huge gap also implied the phenomenon of percolation mentioned above. Since the long-range connection network can create an effective

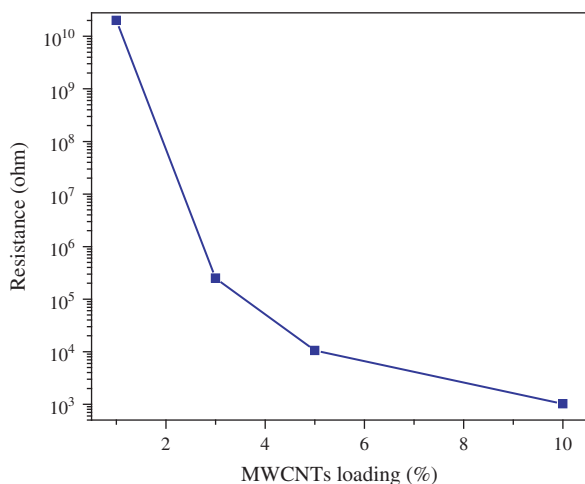


**Fig. 5.** Resistance of the MWCNTs/PU. a, b, c, and d stands for a MWCNTs loadings of 1.0, 3.0, and 5.0 wt%, respectively.

pathway provided almost from MWCNTs for the free electron transporting in the fabricated product, the formation of this interconnection between MWCNTs and PU also attribute to the sharp decrease of the resistance. With the loading of MWCNTs increasing, the interface between MWCNTs and PU has been significantly enhanced, so the accumulations of the charge carriers become easier than lower loading ones. What's more, higher loading can provide a higher possibility for MWCNTs, the conductive materials reach each other and a short distance among the MWCNTs, all of which can further reinforce the transportation of free electrons inside the product and finally decrease the resistance.<sup>9</sup>

The conductivity and resistance of practical applied carbon nanotube is around  $10^2$  to  $10^4 \Omega$  scale.<sup>53, 54</sup> From the graph, the 5% and 10% nanocomposites (enhanced from  $10^5$  to  $10^3$  order of magnitude in resistance) can be developed for the further application in variety fields, which means this work has a strong connection direct to the large scale's application.

### 3.1.5. Thermal Gravimetric Analysis

The thermal stability tests of the MWCNTs/PU had been carried out under both air and nitrogen condition and the thermo grams are demonstrated in Figure 6. There are plenty of researches concluding that with the nano filler such as graphene nanoplatelets,<sup>55</sup> nanoporous poly(methyl methacrylate)-quantum dots,<sup>56</sup> polyaniline,<sup>57</sup> layered double hydroxides<sup>58</sup> and 3-(hydroxyphenylphosphinyl)propionic acid (HPPPA)<sup>59</sup> loaded on the polymer base matrix, the thermal stability had been improved in different degree when comparing to pure polymers. The degradation stages of MWCNTs/PU can be roughly divided into two stages, I and II under air and nitrogen condition, respectively. In stage I the nanocomposites are, to a certain extent, thermally stable (during this region the slight change of weight percentage is attributed to the elimination of the impurity such as water, dust in the product<sup>60</sup>) till the temperature reach the range of 260–270 °C. The next major weight loss of the product occurred at the temperature range of 270–450 °C is due to a large scale thermal degradation of the PU.<sup>22, 23, 61</sup> The decomposition of PU occurs in a two to three step process,<sup>62</sup> marked by arrows in the graph. The depolymerization of PU formed polyol, isocyanate, primary or secondary amine, and olefin and carbon oxide. The degradation of stage I terminated at around 450 °C because the matrix of PU reached its completed decomposition. Since one condition is air and the other is an inert atmosphere, the weight loss of air condition group sample had been directly to 0 while under the nitrogen gas the final would reach the inert composition of MWCNTs with variation of loadings. The phenomenon that with the increase of the MWCNTs the decomposition temperature of the composite slight increase, is obvious to observe from the curve under nitrogen condition, which indicates that

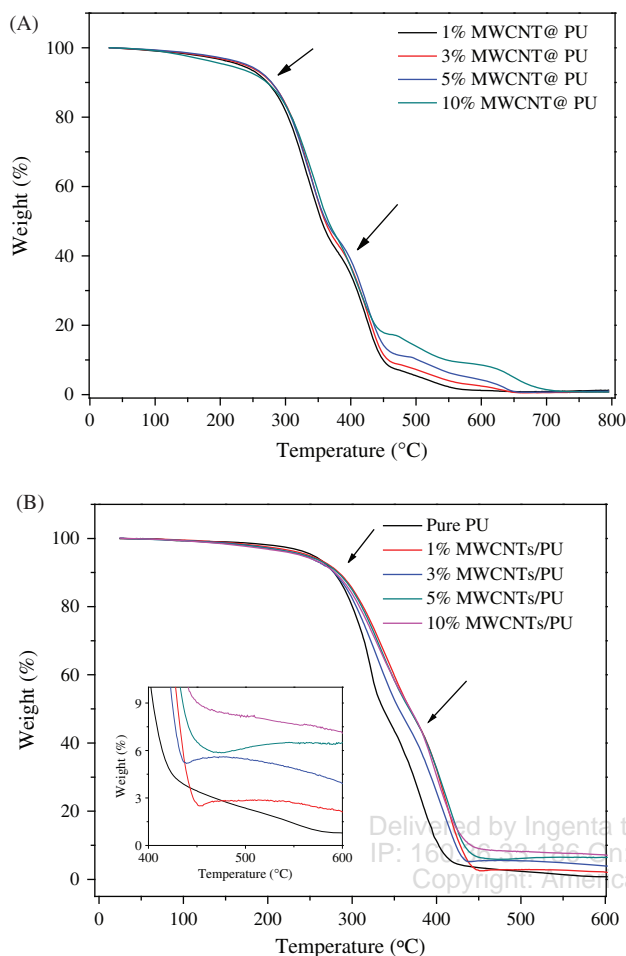


**Fig. 6.** TGA graph of MWNTs/PU under (A) air atmosphere and (B) nitrogen condition.

the loading of MWCNTs formed the restriction for the movement of the PU chains and thus delay the decomposition of the nanocomposites. And this degradation thermo grams results also depicted that the SIP method can form stronger chemical bonds between the loading and the matrix, which can reinforce the thermal stability.<sup>30</sup> All of the above is corresponding to the conclusion that MWCNTs have positive effects on improving the thermal stability of MWCNTs/PU.

### 3.1.6. Strain Sensing Test

Piezoresistivity has been widely investigated with different nanoparticles loadings such as plenty type of CNTs,<sup>11, 63–65</sup> CNFs<sup>8, 9, 66</sup> and so on. The continuous cyclic resistance change corresponding to the stretch and recover responding the continuous cyclic applied external force has been depicted in Figure 7. From these figures, the piezoresistivity phenomenon is easy to observe from the 10 cycles in 1000 cycles per sample. The nanocomposites with 3% loading showed a response to the external applied force and each peak is corresponding to the sawtooth applied strain. Despite few cycle's resistance changed over other

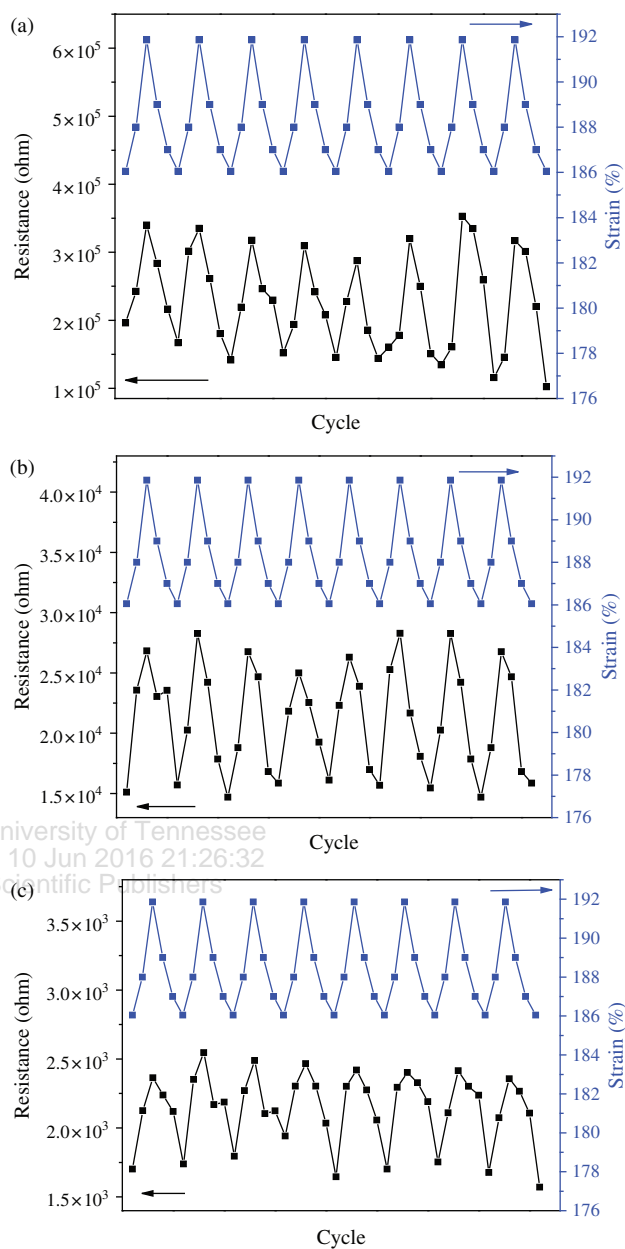


**Fig. 7.** Cyclic strain applied to samples and the instantaneous response of resistance with (a) 3.0, (b) 5.0, and (c) 10.0% wt MWCNTs loading on PU.

cycles, most of the responses demonstrate stable piezoresistivity properties of the MWCNTs/PU nanocomposites. The precise sawtooth length choice is under serious considered since either larger or smaller strain percentage would cause unexpected condition happened similar to some pretreatment, initial cycling.<sup>67</sup> In general, the pretreatment can be separated into three sections: crack opening, elastic deformation and damage accumulation.<sup>9</sup>

The graphs shows that with the loading at 3%, the resistance of the nanocomposites is at around  $10^5$  order of magnitude range while when it comes to 5% loadings MWCNTs/PU, the resistance decreased to  $10^4$  orders of magnitude, indicating an improvement of the conductivity

of the nanocomposites. At each cycle of different loading of nanocomposites, the major peak and major trough are well reflecting the cyclic stress and recover. This can be explained by the stressing procedure deformation and reformation the inner structure of the MWCNTs/PU, which led to an increase of chance for the conductive material MWCNTs connecting or contacting with each other.

The most significant decrease of conductivity occurred in 10% MWCNTs/PU, and the stretch and recover resistance demonstrate a much better responding to the applied force. All the major peaks and major troughs have a better response comparing to 3% and 5% loading nanocomposites, indicating a well functional elastomeric conductive polymer has been synthesized.

#### 4. CONCLUSION

A series of MWCNTs/PU nanocomposites had been synthesized via the SIP method with 1, 3, 5 and 10% loading of MWCNT. By introducing nanoparticles, thermal stability had been improved and conductivity of nanocomposites has also been reinforced. The resistances of the synthesized products were decreased drastically from over  $10^{10}$  straightly down to  $10^3 \Omega$ . 1, 3, and 5% loading MWCNTs achieved positive permittivity while only 10% MWCNTs/PU had a negative permittivity value, which has an acceptable reflect of the percolation effect. Both real and imaginary permittivity, especially in high frequency, higher loading MWCNTs obtained higher value. A controlled range of the strain for the stretch/recovery test had been carried out. The stable performances in these tests also indicate these electrically conductive polymer nanocomposites can be applied as strain sensors with precisely change of the external supplied force to the nanocomposites.

#### References and Notes

- I. Alig, S. M. Dudkin, W. Jenninger, and M. Marzantowicz, *Polymer* 47, 1722 (2006).
- I. Alig, T. Skipa, D. Lellinger, and P. Pötschke, *Polymer* 49, 3524 (2008).
- M. A. Atwater, A. K. Mousavi, Z. C. Leseman, and J. Phillips, *Carbon* 57, 363 (2013).
- J. Cao, Q. Wang, and H. Dai, *Phys. Rev. Lett.* 90, 157601 (2003).
- M. Cao, J. Yang, W. Song, D. Zhang, B. Wen, H. Jin, Z. Hou, and J. Yuan, *ACS Applied Materials and Interfaces* 4, 6949 (2012).
- C. Cha, S. R. Shin, N. Annabi, M. R. Dokmeci, and A. Khademhosseini, *ACS Nano* 7, 2891 (2013).
- M. Chen, Z. Shao, X. Wang, L. Chen, and Y. Wang, *Ind. Eng. Chem. Res.* 51, 9769 (2012).
- W. Chen and X. Tao, *Macromol. Rapid Commun.* 26, 1763 (2005).
- D. L. Cheng, S. N. Lee, C. H. Ho, J. L. Han, and K. H. Hsieh, *J. Phys. Chem. C* 112, 15956 (2008).
- W. Choi and J. Hong, *Ind. Eng. Chem. Res.* 51, 14714 (2012).
- D. J. Cohen, D. Mitra, K. Peterson, and M. M. Maharbiz, *Nano Lett.* 12, 1821 (2012).
- D. Östling, D. Tomaňek, and A. Roseñ, *Physical Review B* 55, 13980 (1997).
- E. Delebecq, J. P. Pascault, B. Boutevin, and F. Ganachaud, *Chem. Rev.* 113, 80 (2013).
- S. Dohn, K. Mølhav, and P. Bøggild, *Sensor Lett.* 3, 300 (2005).
- F. Du, R. C. Scogna, W. Zhou, S. Brand, J. E. Fischer, and K. I. Winey, *Macromolecules* 37, 9048 (2004).
- G. D. M. R. Dabera, K. D. G. I. Jayawardena, M. R. R. Prabhath, I. Yahya, Y. Y. Tan, N. A. Nismy, H. Shiozawa, M. Sauer, G. Ruiz-Soria, P. Ayala, V. Stolojan, A. A. D. T. Adikaari, P. D. Jarowski, T. Pichler, and S. R. P. Silva, *ACS Nano* 7, 556 (2013).
- B. Gao, Y. Chen, M. Fuhrer, D. Glatli, and A. Bachtold, *Phys. Rev. Lett.* 95, 196802 (2005).
- L. M. Gradinaru, C. Ciobanu, S. Vlad, M. Bercea, and M. Popa, *Ind. Eng. Chem. Res.* 51, 12344 (2012).
- H. Gu, Y. Huang, X. Zhang, Q. Wang, J. Zhu, L. Shao, N. Haldolaarachchige, D. P. Young, S. Wei, and Z. Guo, *Polymer* 53, 801 (2012).
- H. Gu, S. Tadakamalla, X. Zhang, Y. Huang, Y. Jiang, H. A. Colorado, Z. Luo, S. Wei, and Z. Guo, *Journal of Materials Chemistry C* 1, 729 (2013).
- Z. Guo, T. Y. Kim, K. Lei, T. Pereira, J. G. Sugar, and H. T. Hahn, *Compos. Sci. Technol.* 68, 164 (2008).
- Z. Guo, S. E. Lee, H. Kim, S. Park, H. T. Hahn, A. B. Karki, and D. P. Young, *Acta Materialia* 57, 267 (2009).
- Z. Guo, S. Park, S. Wei, T. Pereira, M. Moldovan, A. B. Karki, D. P. Young, and H. T. Hahn, *Nanotechnology* 18, 335704 (2007).
- G. Zhong, J. H. Warner, M. Fouquet, A. W. Robertson, B. Chen, and J. Robertson, *ACS Nano* 6, 2893 (2012).
- Q. He, T. Yuan, J. Zhu, Z. Luo, N. Haldolaarachchige, L. Sun, A. Khasanov, Li Y, D. P. Young, S. Wei, and Z. Guo, *Polymer* 53, 3642 (2012).
- N. Hu, Y. Karube, C. Yan, Z. Masuda, and H. Fukunaga, *Acta Materialia* 56, 2929 (2008).
- H. Im, C. Sang, and K. Chang, *Ind. Eng. Chem. Res.* 50, 7305 (2011).
- J. Zhu, S. Wei, L. Zhang, Y. Mao, J. Ryu, P. Mavinakuli, A. B. Karki, D. P. Young, and Z. Guo, *J. Phys. Chem. C* 114, 7 (2010).
- X. Jing, D. Guo, J. Zhang, F. Zhai, X. Wang, L. Chen, and Y. Wang, *Ind. Eng. Chem. Res.* 52, 4539 (2013).
- J. Wu, C. Chen, Y. Zhang, K. Chen, Y. Yang, Y. Hu, J. He, and Z. Wang, *ACS Nano* 6, 4369 (2012).
- C. Li, J. Chen, S. Fan, F. Ko, and F. Chang, *ACS Appl. Mater. Interfaces* 4, 5650 (2012).
- X. Li, R. Zhang, W. Yu, K. Wang, J. Wei, D. Wu, A. Cao, Z. Li, Y. Cheng, Q. Zheng, R. S. Ruoff, and H. Zhu, *Scientific Reports* 2, 870 (2012).
- Y. Li, J. Zhu, S. Wei, J. Ryu, L. Sun, and Z. Guo, *Macromol. Chem. Phys.* 212, 1951 (2011).
- L. Qu, Y. Lin, D. E. Hill, B. Zhou, W. Wang, X. Sun, A. Kitaygorodskiy, M. Suarez, J. W. Connell, L. F. Allard, and Y. P. Sun, *Macromolecules* 37, 6055 (2004).
- G. Magadur, J. S. Lauret, G. Charron, F. Bouanis, E. Norman, V. Huc, C. S. Cojocaru, S. Gomez-Coca, E. Ruiz, and T. Mallah, *J. Am. Chem. Soc.* 134, 7896 (2012).
- E. Minot, Y. Yaish, V. Sazonova, J. Y. Park, M. Brink, and P. McEuen, *Phys. Rev. Lett.* 3, 1 (2014).
- M. Moniruzzaman and K. I. Winey, *Macromolecules* 39, 5194 (2006).
- G. Morral-Ruiz, C. Solans, M. L. Garcia, and M. J. Garcia-Celma, *Langmuir* 28, 6256 (2012).
- K. C. Pradhan and P. L. Nayak, *Advances in Applied Science Research* 3, 3045 (2012).
- P. Dutta, S. Biswas, and S. K. De, *J. Phys.: Condens. Matter* 13, 9187 (2001).
- A. J. Paleo, F. W. J. van Hattum, J. Pereira, J. G. Rocha, J. Silva, V. Sencadas, and Lanceros-Méndez, *Smart Mater. Struct.* 19, 065013 (2010).

42. C. Pang, G. Y. Lee, T. Kim, S. M. Kim, H. N. Kim, S. H. Ahn, and K. Y. Suh, *Nat. Mater.* 11, 795 (2012).
43. A. Pei, J. M. Malho, D. D. Ruokolainen, Q. Zhou, and L. A. Berglund, *Macromolecules* 44, 4422 (2011).
44. C. Robert, J. F. Feller, and M. Castro, *ACS Appl. Mater. Interfaces* 4, 3508 (2012).
45. H. Sardon, L. Irusta, M. J. Fernández-Berridi, M. Lansalot, and E. Bourgeat-Lami, *Polymer* 51, 5051 (2010).
46. K. M. Seeni Meera, R. Murali Sankar, S. N. Jaisankar, and A. B. Mandal, *J. Phys. Chem. B* 117, 2682 (2013).
47. M. K. Shin, J. Oh, M. Lima, M. E. Kozlov, S. J. Kim, and R. H. Baughman, *Adv. Mater.* 22, 2663 (2010).
48. N. K. Shrivastava, S. Suin, S. Maiti, and B. B. Khatua, *Ind. Eng. Chem. Res.* 52, 2858 (2013).
49. P. Slobodian, P. Riha, and P. Saha, *Carbon* 50, 3446 (2012).
50. S. S. Narine, X. Kong, L. Bouzidi, and P. Sporns, *Journal of Oil and Fat Industries* 84, 65 (2007).
51. J. Świergiel and J. Jadżyn, *J. Chem. Eng. Data* 57, 2271 (2012).
52. Z. Tu and Z. OuYang, *Physical Review B* 65, 23 (2002).
53. C. Wang, B. Xie, Y. Liu, and Z. Xu, *ACS Macro Letters* 1, 1176 (2012).
54. Q. Wang, X. Zhang, J. Zhu, Z. Guo, and D. O'Hare, *Chemical Communications* 48, 7450 (2012).
55. S. Wei, J. Sampathi, Z. Guo, N. Anumandla, D. Rutman, A. Kucknoor, L. James, and A. Wang, *Polymer* 52, 5817 (2011).
56. P. A. Withey, V. S. Vemuru, S. M. Bachilo, S. Nagarajaiah, and R. B. Weisman, *Nano Lett.* 12, 3497 (2012).
57. T. Yamada, Y. Hayamizu, Y. Yamamoto, Y. Yomogida, A. Izadi-Najafabadi, D. N. Futaba, and K. Hata, *Nat. Nanotechnol.* 6, 296 (2011).
58. T. Yamada, N. Makiomoto, A. Sekiguchi, Y. Yamamoto, K. Kobashi, Y. Hayamizu, Y. Yomogida, H. Tanaka, H. Shima, H. Akinaga, D. N. Futaba, and K. Hata, *Nano Lett.* 12, 4540 (2012).
59. B. Yang, W. M. Huang, C. Li, and L. Li, *Polymer* 47, 1348 (2006).
60. X. Zhang, Q. He, H. Gu, H. A. Colorado, S. Wei, and Z. Guo, *ACS Applied Materials and Interfaces* 5, 898 (2013).
61. X. Zhang, S. Wei, N. Haldolaarachchige, H. A. Colorado, Z. Luo, D. P. Young, and Z. Guo, *J. Phys. Chem. C* 116, 15731 (2012).
62. D. Zhu, J. Zhang, Y. Bin, C. Xu, J. Shen, and M. Matsuo, *J. Phys. Chem. A* 116, 2024 (2012).
63. J. Zhu, H. Gu, Z. Luo, N. Haldolaarachchige, D. P. Young, S. Wei, and Z. Guo, *Langmuir* 28, 10246 (2012).
64. J. Zhu, S. Wei, I. Y. Lee, S. Park, J. Willis, N. Haldolaarachchige, D. P. Young, Z. Luo, and Z. Guo, *RSC Advances* 2, 1136 (2012).
65. J. Zhu, S. Wei, J. Ryu, and Z. Guo, *J. Phys. Chem. C* 115, 13215 (2011).
66. J. Zhu, S. Wei, L. Zhang, Y. Mao, J. Ryu, N. Haldolaarachchige, D. P. Young, and Z. Guo, *J. Mater. Chem.* 21, 3952.
67. J. Zhu, X. Zhang, N. Haldolaarachchige, Q. Wang, Z. Luo, J. Ryu, D. P. Young, S. Wei, and Z. Guo, *J. Mater. Chem.* 22, 4996 (2012).

Delivered by Ingenta to: University of Tennessee  
IP: 160.36.33.186 On: Fri, 10 Jun 2016 21:26:32  
Copyright: American Scientific Publishers